doi:10.1038/nature12470

Supplementary Figure 1: Mosaic of the IBIS/ISGRI field of view around IGR J18245–2452 obtained by using Science Windows 83-107 collected in the direction of the source during satellite revolution 1276 (20–40 keV energy range).

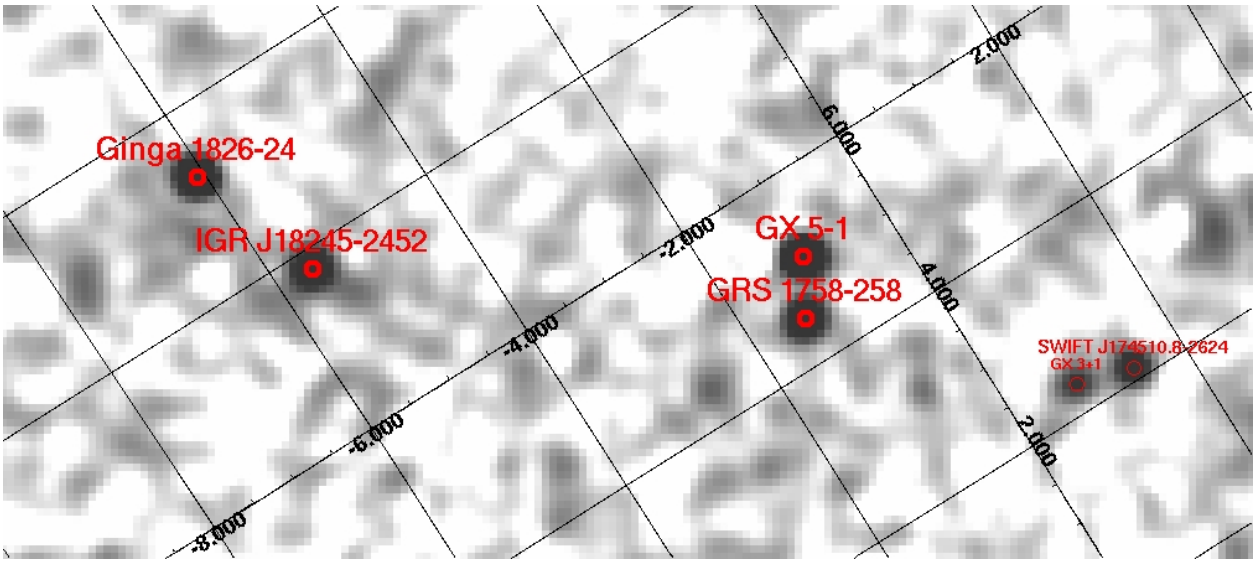

Supplementary Figure 2: Peak-to-peak amplitude of the first harmonic measured during XMM-Newton OBS 1 and OBS 2, normalised to the average count rate, and 0.5-10 keV EPIC pn count rate evaluated over 2 ks long intervals. The dashed red line is the best fit linear regression between the two variables. Typical errors bars are shown for sample points.

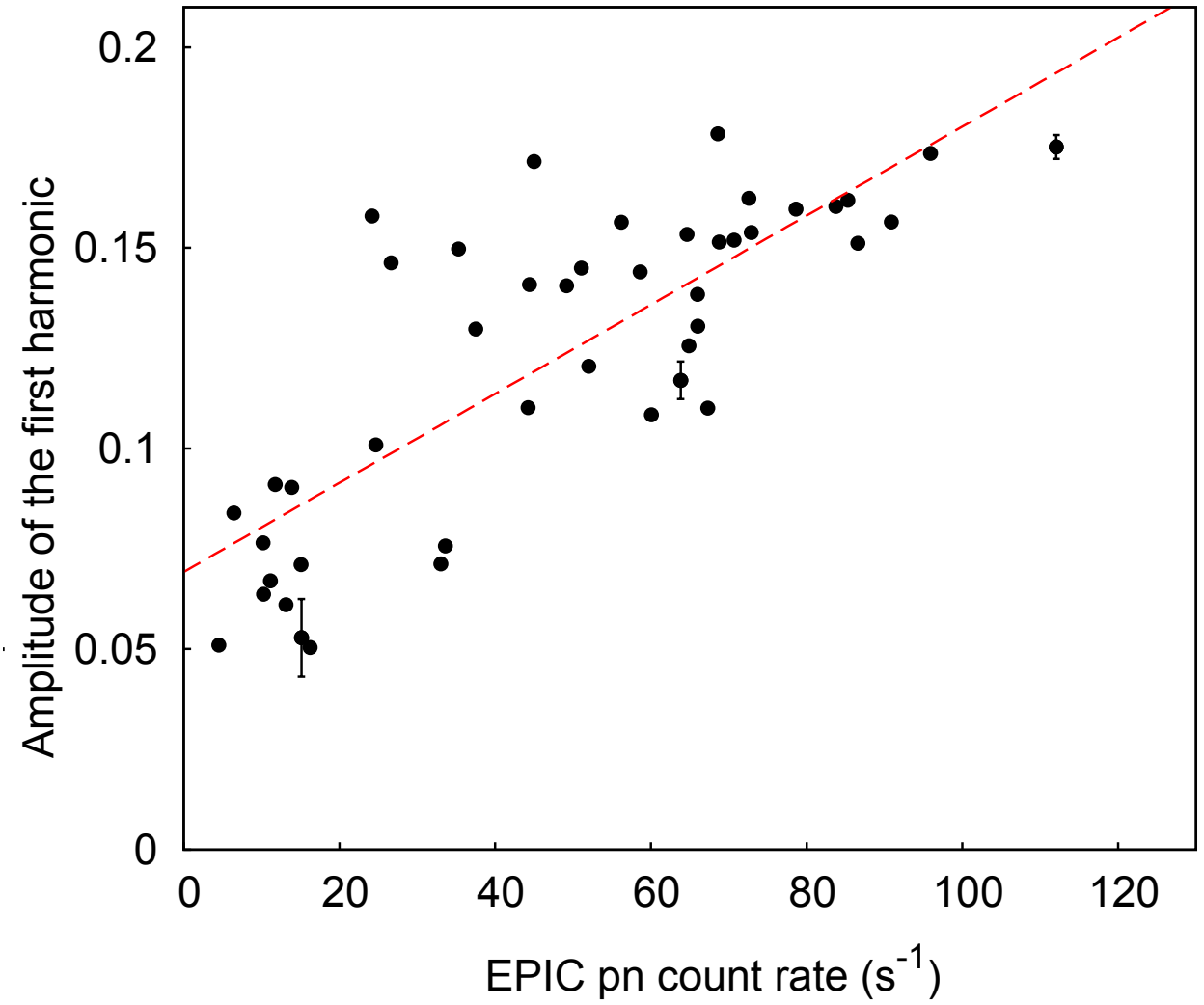

Supplementary Figure 3: X-ray spectrum observed by the EPIC pn camera during OBS 1 and OBS 2 (red and blue points, respectively). The best fit model is plotted as a black solid line, the disc emission, the Comptonized emission, the iron emission feature, and the feature of calibration origin, are plotted as an orange, green, grey and magenta dashed lines, respectively (top panel). Residuals in units of σ of the observed spectra, with respect to the best fit model (bottom panel).

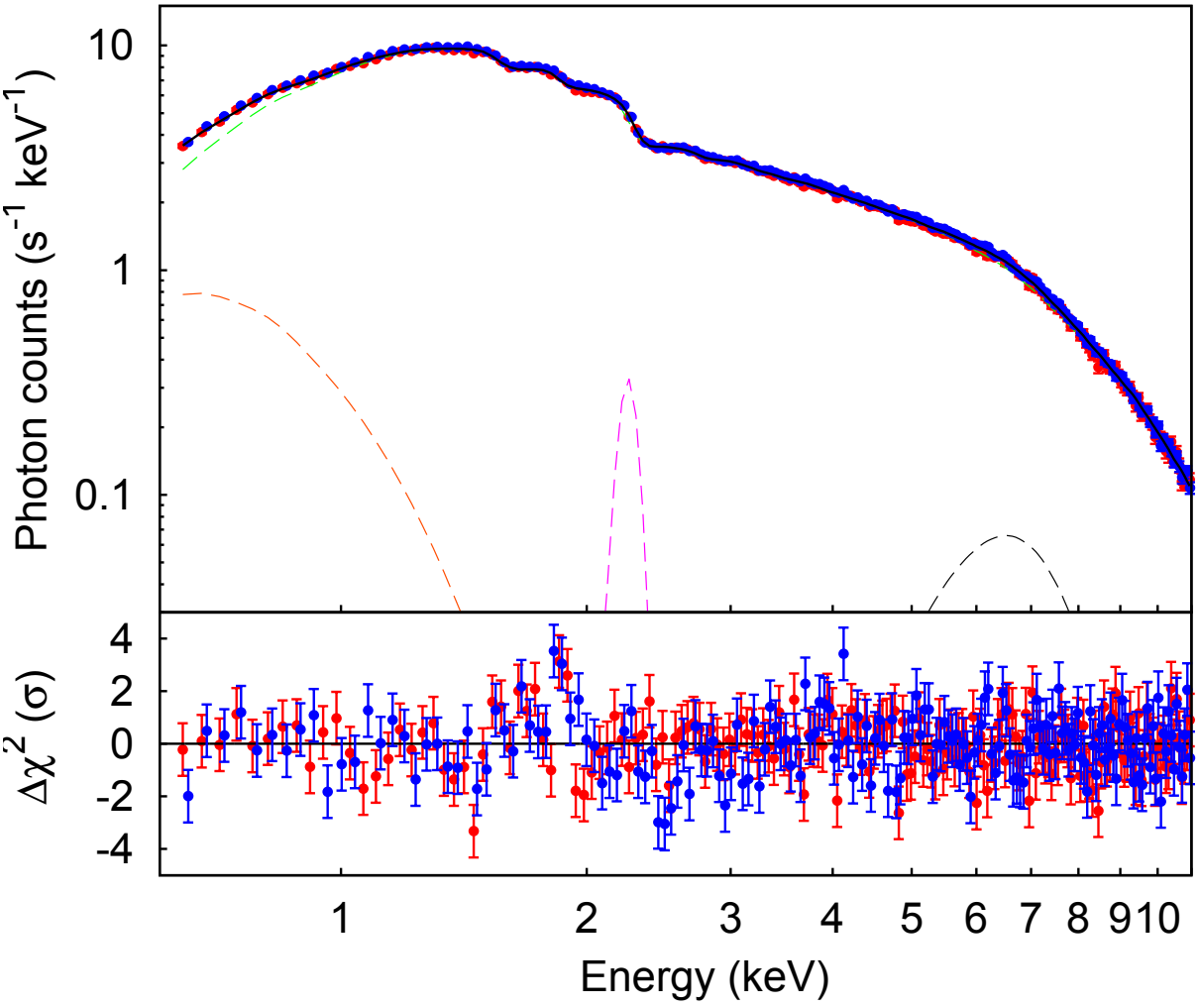

Supplementary Figure 4: Thermonuclear burst observed by XRT, with the best fit exponential decay model plotted as a red dashed line. Blue points show the temperature of the black body which we used to model the XRT 0.5-10 keV spectra, and refer to the right axis. The inset shows the pulse profile observed at the spin period of the source, during the interval marked by the horizontal thick bar.

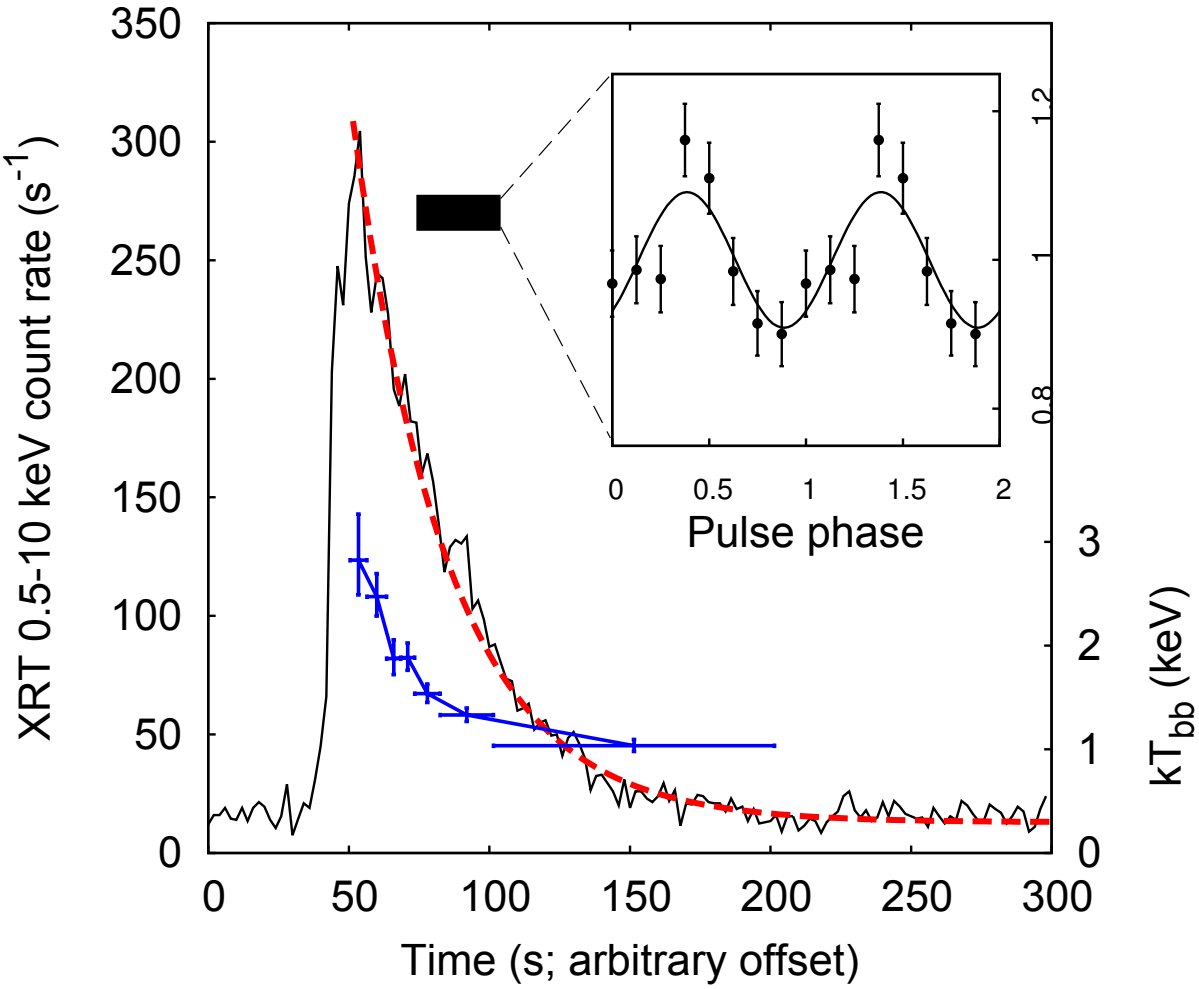

Supplementary Figure 5: Chandra ACIS–S light curve of the August 2008 observations, when the source was undergoing an X-ray outburst. Light curve is background subtracted, binned at 1000s and in the 0.3–10 keV energy range. Data were not available during the interval between 1.5×10^5 and 2.7×10^5 s, since the beginning of the first observation.

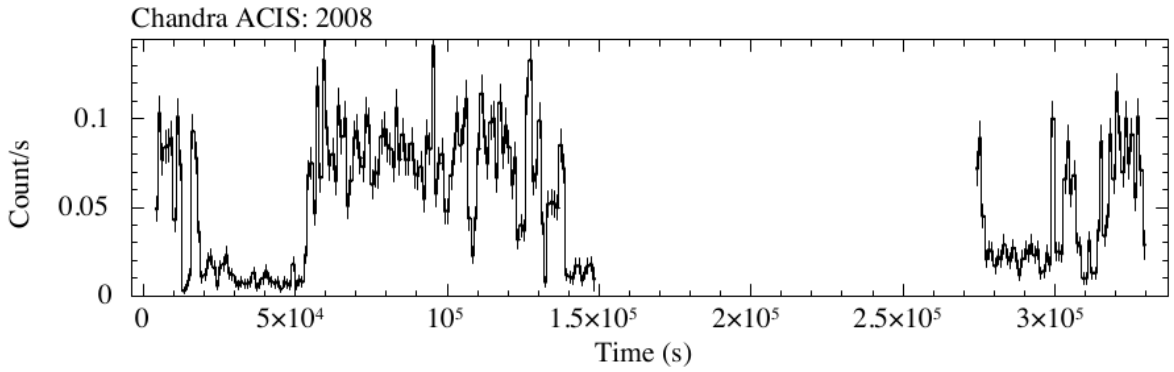

Supplementary Figure 6: ACIS–S spectra of all *Chandra* observations of IGR J18245–2452 (4 July 2002, cyan triangles; 4 August 2002, light blue triangles; 9 September 2002, blue triangles; 7 August 2008, red triangles; 10 August 2008, orange triangles; see Supplementary Table 2 for details) modelled with an absorbed power-law model (top panel) and residuals with respect to the best fitting absorbed power-law model (bottom panel).

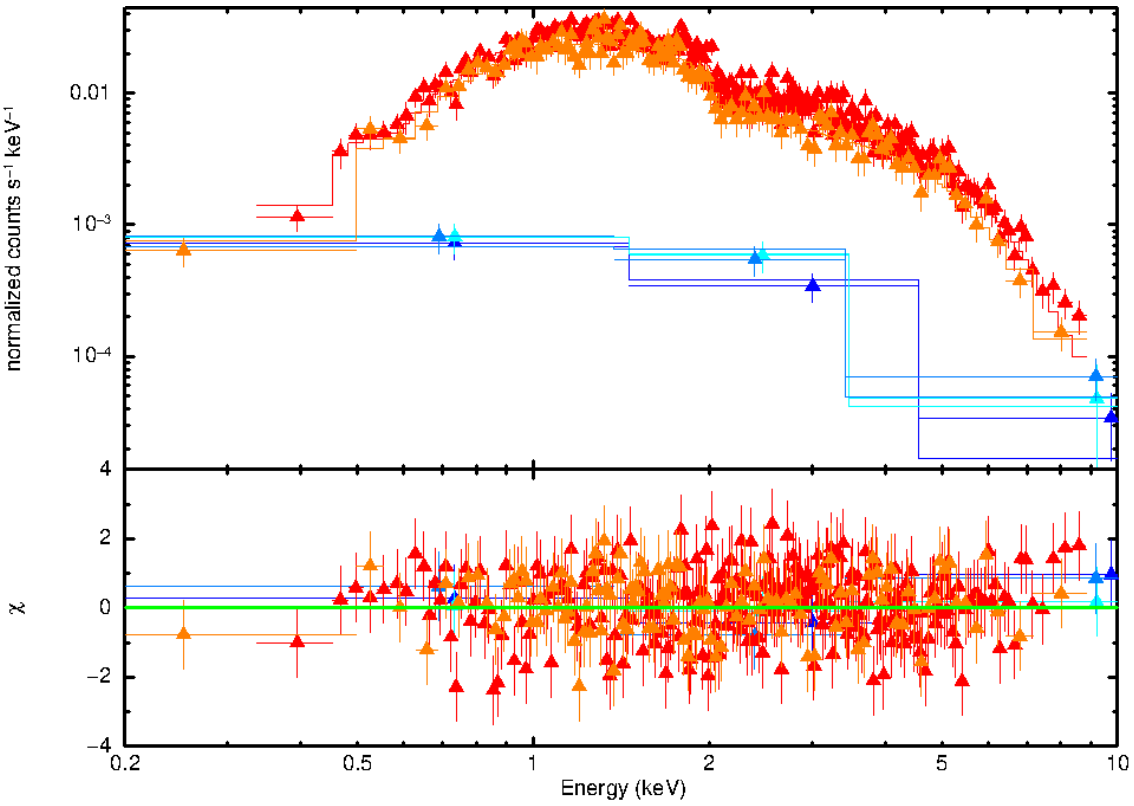

1 INTEGRAL detection of IGR J18245–2452

IGR J18245–2452 was first detected[31] by the hard X-ray imager IBIS[32] using the ISGRI[33] detector on-board INTEGRAL[34], on 28 March 2013, during observations of the Galactic Center. We analysed the corresponding data (pointings from 83 to 107 in satellite revolution 1276) by using the Off-line Science Analysis software provided by the Integral Science Data Centre. The source was detected in the ISGRI mosaicked image at a significance level of 21σ in the 20–40 keV energy band and 15σ in the 40–80 keV energy band (see Supplementary Figure 1). The best source position was obtained at RA=276.14°, Dec=24.88° (J2000), with an associated uncertainty of 1.4′ at 90% confidence level, well within the globular cluster M28. During the first detection of the source, its flux estimated from the ISGRI data was 9×10^{-10} erg cm^{-2} s^{-1} in the 20-100 keV energy band, during an effective exposure time of 32 ks, corresponding to a luminosity of 3×10^{36} erg s^{-1}, at a distance[35] of 5.5 kpc. The source was outside the field of view of the JEM-X instrument[36], sensitive in the 3–30 keV energy band, during the entire observation.

2 XMM-Newton observations of IGR J18245–2452

Following the detection of IGR J18245–2452 by INTEGRAL, we obtained two target of opportunity observations with the X-ray Multi-Mirror Mission[37] (XMM-Newton), starting on 3 April 2013, at 23:49 (Obs. ID 0701981401, OBS 1, hereafter) and 13 April at 06:25 (Obs. ID 0701981501,

OBS 2), and lasting 26.7 and 67.2 ks, respectively (all the epochs are given in the Coordinated Universal Time). The European Photon Imaging Camera (EPIC) pn[38] was operated in fast timing mode, the two EPIC MOS cameras[39] in small window imaging mode, and the Reflection Grating Spectrometers[40] (RGS) in standard spectroscopy mode. A thick blocking filter was used to shield the EPIC cameras from contamination of optical light. All the data were reduced by using the latest version of the XMM-Newton Science Analysis Software (SAS ver. 13). The average count rates observed by the EPIC pn, EPIC MOS1, EPIC MOS2, RGS1 and RGS2 (in their first order of dispersion) during the first (second) observations were 68.1 (71.0), 11.8 (11.7), 11.6 (11.5), 0.68 (0.86) and 0.69 (0.88) s^{-1}, respectively. Since the source is detected also at energy larger than 10 keV, we built a 0.5–10 keV light curve from a background region falling in one of the outer chips of the EPIC MOS cameras which was not pointing the source, in order to ensure that soft proton flares of Solar origin did not contaminate the observations.

Timing Analysis. The timing observing mode of the EPIC pn camera has a timing resolution of 29.52 μs. This resolution is achieved by losing spatial information along one of the axes of the CCD. To extract the source emission, we considered X-ray photons falling within 86.1″ from the source position measured along one of the pointing axes (corresponding to a full width of 21 EPIC pn pixels), and containing 95% of the energy at every observed wavelength. The background emission was extracted from a region of width 12″ (corresponding to 3 EPIC pn pixels).

Although X-ray pulsations from several accreting millisecond pulsars have already been observed by XMM-Newton[41–45], this is the first time that pulsations from an accreting millisecond

pulsar have been discovered by this observatory. In order to perform a timing analysis of the signal, the times of arrival of X-ray photons were converted to the Solar System barycentre, by using the position determined by Chandra (see Sec. 4 below) and Solar System ephemerides JPL DE405. We derived a zeroth order orbital solution by measuring the spin period in 2-ks long intervals through an epoch folding technique[46], and modelling the orbital modulation affecting the values obtained. To assess the significance of any detection we considered that in the absence of any periodic signal, the variance of a folded profile follows a χ^2_{n-1} distribution with $n-1$ degrees of freedom, where n is the number of phase bins used to sample the signal period[46] ($n = 12$ in this case). We then used the preliminary determination of the pulsar orbital parameters to convert the photon arrival times to the line of nodes of the binary system. This procedure was iterated until the spin period was observed to be constant throughout the observations. To further refine the parameters, we then folded data around the current best estimate of the spin period, considering 12 phase bins and describing the pulse profile with two harmonic components. The variation of the phase of the first harmonic over time was modelled in terms of the difference between the orbital and spin parameters used to correct the photon arrival times, and the actual ones[47]. The procedure was iterated until no significant corrections to the parameters were found within the uncertainties[48]. We checked that the phase difference between the first and second harmonic component was compatible with a constant.

The amplitude of the harmonic component at the fundamental frequencies varied between 18% and the non detection, in strong positive correlation with the count rate observed in the 0.5–10 keV (see Supplementary Figure 2). The Spearman's rank correlation coefficient evaluated from the observed count rate and amplitude is $\rho = 0.79$ for 45 points, implying a probability of less than

10^{-10} that the two variables are not correlated.

Spectral Analysis. We built an X-ray spectrum of the emission observed by the EPIC pn by excluding the two brightest columns of CCD pixels (RAWX=37–38), to avoid the effect of photon pile up during the time intervals in which the count rate was the highest. Spectral bins were grouped to over-sample the effective instrument resolution by a factor not larger than three. Response matrices were built following the guidelines provided by the XMM-Newton calibration technical notes. The two observations were modelled simultaneously as they had a compatible average spectral shape. We modelled the 0.6–11 keV observed spectra with an accretion disk spectral component[49] (`diskbb` in the terminology used by the spectral fitting routine used, Heasarc's XSPEC v.12.8.0), and with the emission produced by a thermal distributions of electrons which Compton up-scatter soft seed X-ray photons, with a black-body spectral shape[50,51] (`nthcomp`). A similar spectral decomposition well described the X-ray spectra shown by accreting millisecond pulsars[52], observed by the EPIC pn camera[41–45]. The temperature of the electron cloud was fixed at 50 keV, outside the energy band observed by the EPIC pn camera, following the values usually observed at higher energies from accreting millisecond pulsars[52,53] ($kT_e \gtrsim 20$ keV). Absorption of the interstellar medium was modelled according to the Tuebingen-Boulder model (Wilms, J. et al. 2011, in preparation, http://pulsar.sternwarte.uni-erlangen.de/wilms/research/tbabs/). The value of the absorption column was fixed to the value measured by fitting the average spectra observed by the RGS 1 and 2 with an absorbed power law ($N_{\rm H} = 0.31(1) \times 10^{22}$ cm^{-2}); solar abundances were considered. A broad Gaussian emission feature centred at an energy compatible with iron K-α emission (6.4–6.97 keV), and a narrow emission feature most probably

due to calibration residuals around the edge of Au (Guainazzi, M. et al. 2012, available from http://xmm2.esac.esa.int/docs/documents/CAL-TN-0083.pdf), decreased significantly the variance of model residuals. The best-fit parameters obtained modelling the spectra observed during the two XMM-Newton are given in Table 1, while the observed spectrum and residuals are plotted in Supplementary Figure 3.

The position. To determine the source position we accumulated images from the EPIC MOS1 and MOS 2 in the energy bands 0.5-1 keV, 1-2 keV, 2-4.5 keV, and 4.5-12 keV, during the time intervals in which the source count rate was < 1.5 s^{-1} (0.5–10 keV). This selection prevented pile-up and resulted in a total effective exposure time of 5.7 and 13.8 ks for the two instruments in OBS 1 and OBS 2, respectively. We created an exposure map using the attitude information to mask out the regions of the detector where not enough exposure was available, and performed a first localisation of the sources in the raw images using the sliding box method[54]. A background map was then produced from the previous images by removing the identified sources (taking into account the local instrument point spread function), and used together with previous products to perform a second optimised source localisation. The data of the two MOS cameras in the two observations and different energy bands provided a total of 16 independent estimates of the source position. By averaging such estimates we obtained a position of RA=$18^h24^m32.36^s$ Dec=$-24°52'06.3''$. We added in quadrature the 1σ uncertainty we derived with the described analysis ($1.5''$) to the systematic error reported in the XMM catalogue[54] ($1.0''$), to obtain a total uncertainty of $1.8''$ (1σ confidence level). The error circle at a 3σ confidence level is plotted as a white circle in Fig. 3 of the main body of the Letter.

Table 1: Average spectral parameters of IGR J18245–2452.

Absorption column ($N_{\rm H}$)$^{(a)}$	$0.31(1) \times 10^{22}$ cm^{-2}
Inner disk temperature ($kT_{\rm in}$)	$0.13(1)$ keV
Apparent inner disk radius ($R_{\rm in}\sqrt{\cos i}$)$^{(b)}$	52^{+19}_{-13} km
Seed photon temperature ($kT_{\rm soft}$)	$0.31(1)$ keV
Asymptotic power-law photon index (Γ)	$1.41(1)$
Electron temperature ($kT_{\rm e}$)	50 keV
Energy of iron line ($E_{\rm Fe}$)	6.74 ± 0.11 keV
Width ($\sigma_{\rm Fe}$)	$1.1(2)$ keV
Normalisation ($N_{\rm Fe}$)	$4.8(1) \times 10^{-3}$ cm^{-2} s^{-1}
Energy of line of calibration origin ($E_{\rm cal}$)	$2.24(1)$ keV
Normalisation ($N_{\rm cal}$)	$1.3(2) \times 10^{-4}$ cm^{-2} s^{-1}
Unabsorbed flux (0.5–10 keV; F_1)$^{(c)}$	$3.08(1) \times 10^{-10}$ erg cm^{-2} s^{-1}
Unabsorbed flux (0.5–10 keV; F_2)$^{(d)}$	$3.17(1) \times 10^{-10}$ erg cm^{-2} s^{-1}
Reduced chi-squared, χ^2_ν(d.o.f.)	$1.27(355)$

Parameters based on spectral modelling of the two observations of IGR J18245–2452 performed by the EPIC pn camera. Values in parentheses are the uncertainties on the last significant digit, evaluated at a 90% confidence level.

$^{(a)}$ The value of the interstellar absorption column density was measured by modelling the spectra observed by the two units of the RGS with an absorbed power law. This value was held fixed when fitting the EPIC pn spectra. We used abundances and photoelectric cross-sections from ref. 54 and 55, respectively.

$^{(b)}$ The disk apparent radius depends on the disk inclination, i, and was evaluated for a distance of 5.5 kpc (ref. 35).

$^{(c-d)}$ Unabsorbed flux during OBS 1 and OBS 2, respectively.

3 Swift observations of IGR J18245–2452

After the initial arc-second localisation with the X-ray Telescope[55] (XRT) on-board Swift[56], the source triggered the Burst Alert Telescope[57] (BAT) on 30 April 2013 at 02:22:21 UT and subsequently at 15:10:37 UT and 15:17:33.61 UT. Several observations with XRT were obtained starting from 30 April, including a intensive one between the BAT triggers (Obs. Id 32787) and a long term one (Obs. Id 32785). Analysis of the XRT observation performed on 30 April yielded a determination[58] of the position of the source RA=$18^h24^m32.24^s$ Dec=$-24^\circ52'05.7''$, with an uncertainty of 3.5$''$ at a 90$\%$ confidence level, compatible with that determined by ref. 59, and those measured by EPIC MOS (see Sec.2 above), Chandra (see Sec. 4 below), and ATCA (see Sec. 5). The 0.5–10 keV flux corrected for absorption attained a maximum level of $9.6(1) \times 10^{-10}$ erg cm^{-2} s^{-1} during an observation starting on 30 March 2013 (Obs.ID 00552369000), with a spectral distribution well described by a power law with index $\Gamma = 1.35 \pm 0.04$. The last detection was obtained during a 0.8-ks observation performed on 1 May 2005 (Obs. ID 00032785021), with an observed flux of $(1.6 \pm 0.4) \times 10^{-12}$ erg cm^{-2} s^{-1}. This value of the flux was estimated assuming a $\Gamma = 2.5 \pm 0.6$, power-law shaped spectrum, as derived summing all Swift observations taken in the week starting from 21 April 2013. We note that a flux contamination of $\approx 3 \times 10^{-13}$ erg cm^{-2} s^{-1} is expected to be produced by other unresolved source in M28, among which PSR B1821-24 gives the largest contribution[60,61]. Details of a sample of Swift/XRT observations are given in Supplementary Table 3.

During an observation that started on 7 April at 20:32 (Obs. ID 00032785005), a bursting

event was observed[45,62] by the XRT when it was observing in windowed timing mode with a temporal resolution of 1.78 ms. The burst profile has the typical shape observed from thermonuclear explosions taking place at the surface of the neutron star[63], with a fast rise of $\lesssim 10$ s and an exponential decay on a time scale of 38.9 ± 0.5 s (see red dashed line in Supplementary Figure 4). We performed a time resolved analysis of the emission observed by XRT during the burst. We fit all spectra with a black body emission absorbed by the interstellar medium, fixing the value of the absorption column to that indicated by the XMM-Newton analysis (see Tab. 1). We used the emission observed by XRT during a 100-s interval before the burst as a background to the burst emission. The values of temperature we observed are plotted as blue dots in Supplementary Figure 4. The temperature decay observed during the burst tail agrees with the cooling expected after the thermonuclear burning[63], confirming the nature of the observed event.

We used the Chandra pulsar position (see Sec. 4, below) and orbital parameters determined from the XMM-Newton observations (see Sec.2 and Table 1 in the main body of the Letter) to report the photons arrival times to the Solar system Barycentre and to the pulsar line of nodes. We divided the first 160 s since the burst onset into four intervals, finding in the second one a significant signal at the pulsar period, with an amplitude of $13 \pm 2\%$ (see the inset of Supplementary Figure 4). After taking into account the number of trials made, the detection is significant at a 3.2σ level. A signal with an amplitude of $6.0 \pm 1.2\%$ is detected during the 740 s observed by XRT before the burst onset. The increase of the signal amplitude indicates that the signal observed during the burst is related to this event (i.e., it is a burst oscillation[64]) and is not coming from a background source present within the field of view of XRT. Similar results were reported by ref. 65 and 66.

We also searched for oscillations during the other observations performed by Swift, and found a signal significant above a 3σ confidence level during the observation starting on 30 March 2013 (Obs. ID 00552369000), with an amplitude of $7.4 \pm 1.9\%$.

4 Chandra observations of IGR J18245–2452

The *Chandra* X-ray observatory observed IGR J18245–2452 on 29 April 2013, starting from 00:24:14 for 53 ks, via Director's Discretionary Time. The observations were performed using the High Resolution Camera[67] (HRC–S) in timing mode, which has a $6'' \times 30''$ field of view with a 16-μs timing resolution, but no spectral information. Data were reduced with the CIAO 4.5 software. We first checked the data for the presence of solar flares and extracted a new observation-specific bad-pixel file. We then ran a degap correction, and cleaned the image for the hot pixels.

The new Chandra image of the M28 globular cluster was compared to the several observations of the field performed by Chandra during the past decade (see Table 2 for a complete list, and Fig. 3 of the main body of the Letter for a comparison). We identified one source (source 23 from ref. 60) to be an order of magnitude brighter than in many previous Chandra observations. We used the CIAO tools `wavdetect` and `celldetect` to infer a good position for the transient source, which was RA=$18^h\ 24^m\ 32.527^s$, Dec=$-24^\circ\ 52'\ 08.58''$, with $0.6''$ uncertainty (at 1-σ confidence level, inferred from a $0.3''$ and a $0.5''$ statistical and pointing accuracy, respectively). The position of this transient source is consistent within a 3-σ confidence level with the XMM–Newton (see Sec. 2), Swift (see Sec. 3) and ATCA position (see Sec. 5 below) of IGR J18245–2452 (see

Fig. 3 of the main body of the Letter). We therefore identify it as the accreting X-ray pulsar, IGR J18245–2452.

We have extracted the source events from a 2″ region around the position of the source (and background spectra far from the globular cluster). In this Chandra observation the source had a count rate of 0.0251(5) counts per second (see Tab. 2), which assuming the spectral shape that IGR J18245–2452 had in the closest Swift XRT observation (a power-law with $\Gamma = 2.5 \pm 0.6$; derived summing all Swift observations taken in the week starting from 21 April 2013), leads to a 0.5–10keV observed flux $\sim 4 \times 10^{-13}$ erg cm^{-2} s^{-1}.

We searched for a coherent signal at the spin period of the source in the time series corrected for the spacecraft and orbital motion, and converted to the Solar System Barycentre. No signal was detected at a confidence level of 3σ, with an upper limit of 17% on the pulse amplitude, derived following the prescription given by Vaughan et al. [65]. Pulsations at an amplitude lower than such a value were observed during most of the XMM-Newton observations (see Supplementary Figure 2), when the source was brighter by three orders of magnitude. The non-detection of pulsations does not rule out that the X-ray emission of IGR J18245–2452 was pulsed during the Chandra observation, at a level similar to that previously seen.

We have re-analysed all archival observations performed by Chandra in the past decade to identify and follow the flux evolution of the source. Timing and spectral data were always extracted from a 2″ region around the position of the source. A previous X-ray outburst of IGR J18245–2452 is detected during the August 2008 observations performed with the Advanced CCD Imaging

Spectrometer[68] (ACIS; see Fig. 3 of the main body of the Letter). The light curve of this previous outburst shows a strong variability on many timescales (see Supplementary Figure 5). The most noticeable event is a total quenching of the X-ray emission for a timescale of $\sim$10 hrs, compatible with a complete orbital period. We did not detect a significant energy dependency of the light curve shape.

Spectra were extracted from all the archival observations performed with ACIS-S (all taken in VFAINT mode), which have a good spectral and imaging resolution, but a 3.2 s timing resolution, insufficient to search for millisecond pulsations. We found a good fit ($\chi^2_\nu = 0.91$ with 378 degrees of freedom) when modelling all ACIS-S spectra together with an absorbed power-law model (leaving the photoelectric absorption parameter, N_H, tied to be the same for all spectra). We found a flux variability of more than one order of magnitude between the 2002 and the 2008 observations of IGR J18245–2452 (see Supplementary Figure 6 and Tab. 2). In particular, we found $N_H = 0.26(2) \times 10^{22}\,\mathrm{cm}^{-2}$ (with abundances and photoelectric cross-sections from ref. 69 and 70, respectively), a stable photon index $\Gamma \sim 1.5$, and a 0.5–10 keV flux varying from 2.4 to $64 \times 10^{-14}\,\mathrm{erg\,cm^{-2}\,s^{-1}}$ (all errors are at 90% confidence level).

5 ATCA observations of IGR J18245–2452

On 2013 April 5 we observed IGR J18245–2452 with the Australia Telescope Compact Array (ATCA), at 9 and 5.5 GHz simultaneously. The data were analysed with the Miriad package distributed by ATNF[71]. Only one source was detected in the inner core of the cluster, at a significance

Table 2: *Chandra* observations of the Globular Cluster M28.

Instrument	ObsID	Date	Exposure time (ks)	Source Count/s[a]	Γ[b]	Flux[c]
ACIS–S	2684	2002-07-04	12.7	0.0029(6)	1.5(0.7)	3.1(9)
ACIS–S	2685	2002-08-04	13.5	0.0030(5)	1.4(0.7)	3.5(9)
ACIS–S	2683	2002-09-09	14.1	0.0025(4)	1.6(0.7)	2.4(7)
HRC–S	2797	2002-11-08	48.3	0.0036(5)	1.5 fix	4.8
HRC–S	6769	2006-05-27	40.9	0.0036(5)	1.5 fix	4.8
ACIS–S	9132	2008-08-07	142.3	0.0563(6)	1.51(5)	64(2)
ACIS–S	9133	2008-08-10	54.5	0.04393(9)	1.58(7)	47(2)
HRC–S	15645	2013-04-29	53.0	0.0503(8)	2.5 fix	41

[a] We report the HRC–S counts converted in ACIS-S counts for an easier comparison. The HRC–S original count rate is 0.0012(3) for the first and second HRC–S observation, and 0.0251(5) for the more recent one.

[b] Absorption column density is $N_H = 0.26(2) \times 10^{22}\,\mathrm{cm}^{-2}$.

[c] Absorbed, in the 0.5–10 keV energy range, and in units of $10^{-14}\,\mathrm{erg\,cm^{-2}\,s^{-1}}$. HRC–S fluxes are estimated assuming the source N_H and a power-law spectrum with $\Gamma = 2.5$.

level of nearly 20σ in both frequencies, allowing for an accurate determination of its position at RA=$18^h24^m32.51^s$ Dec=$-24^\circ52'07.9''$, with a 90% confidence error of 0.5″. This position is consistent with that determined by Chandra (see Sec. 4 and Fig. 3 of the main body of the Letter). The mean flux density of this source was 0.75±0.04 (0.62±0.03) mJy at 9 (5.5) GHz respectively, yielding a mean spectral index of 0.4 ± 0.2. During the first 90 minutes of the observation, the source was strongly variable, reaching up to 2.5 times the mean flux density.

The spectral properties of the ATCA source are similar to those observed from other accreting millisecond pulsars[72], and interpreted in terms of emission originating from shocks within material ejected by the X-ray pulsar. Besides PSR J1824–2452I=IGR J18245–2452, which was powered by accretion at that moment, none of the other rotation-powered pulsars in the cluster were detected during the ATCA observation.

6 Parkes radio telescope observations of PSR J1824–2452I

IGR J18245–2452 was observed three times with the 64-m Parkes radio telescope in 2013 April/May (see Supplementary Table 3). We used the position determined by Chandra (see Sec. 4 above). The observations were carried out using simultaneously the Berkeley-Parkes Swinburne Recorder (BPSR) and the Parkes Digital Filterbank (PDFB4) in search mode, for the first epoch, and BPSR and the analogue filterban (AFB), for the subsequent ones. The backends were operating at central frequencies of 1382 MHz (BPSR) and 1369 MHz (PDFB4 and AFB) , over bandwidths of 400 and 256 MHz respectively, subdivided in 1024 frequency channels (512 for AFB). The total usable

bandwidth for BPSR, after removal of a known interference from the Thuraya3 satellite, is 350 MHz.

The resulting time series, 2-bit sampled every 64 μs for BPSR and PDFB4, and 1-bit sampled every 80 μs for AFB, were folded with the `dspsr` package[73] using the X-ray ephemeris presented in this work and using a value of the dispersion measure[74] of 119 pc cm^{-3}. PSR J1824–2452I was detected in two of three Parkes observations (see Supplementary Table 3). In the case of the non-detection, the flux density upper limit derived using the radiometer equation modified for pulsars[75] is $S_{min} = 0.067$ mJy for a signal with a signal-to-noise ratio SNR=8 and a pulse duty cycle of 15 per cent. We caution that Parkes non-detection, as well as other radio non-detections presented below, cannot be taken as strong evidence that the radio pulsar was not active. PSR J1824–2452I is well known to eclipse in the radio[61], particularly around superior conjunction, and this is likely the cause of at least some of the radio non-detections presented in Supplementary Table 3. Though there is no published flux density for PSR J1824–2452I, given its comparable brightness to other pulsars in M28, it is likely that if the source was emitting as a radio pulsar during these observations that it would be at the threshold of detectability during this 64-m Parkes radio telescope observation - especially if the signal was further perturbed by intra-binary material, as in similar systems. Therefore, we consider these observations only moderately constraining as to whether the source was emitting as a radio pulsar at this epoch.

7 Westerbork Synthesis radio telescope observations of PSR J1824–2452I

We observed IGR J18245–2452 during four sessions in 2013 May using the Westerbork Synthesis radio telescope (WSRT). The pointing position was $18^h\,24^m\,32.496^s$, $24^\circ\,52'07.799''$. We used WSRT in the tied-array mode (gain, G = 1.2 K/Jy), combining 13 of the individual 25-m dishes in phase and recording with the PuMaII pulsar data recorder[76]. We recorded a 160-MHz bandwidth and coherently de-dispersed and folded the data offline using the `dspsr` package[73] and the X-ray-derived ephemeris presented here. PSR J1824–2452I was just barely detected in one of four WSRT observations (see Supplementary Table 3). Using the radiometer equation modified for pulsar signals[75], we can place a flux density limit of $S_{1400} = 0.08$ mJy on radio emission from the pulsar in the case of the non-detections. Note that the flux of PSR J1824–2452I is very close to WSRT's detection threshold and, as mentioned above, the radio pulsar may simply have been eclipsed in the case of non-detections.

8 Green Bank Telescope observations of PSR J1824–2452I

We observed IGR J18245–2452 during seven sessions in 2013 May using the Green Bank Telescope (GBT). The Chandra position presented here was used for pointing, and data were acquired using the GUPPI data recorder[77] in a 800-MHz band centered at 2.0GHz. PSR J1824–2452I was detected in two of seven observations (see Supplementary Table 3). Flux density limits in the case of non-detections are $S_{2000} \lesssim 20\mu$Jy, but come with the same caveats about eclipsing as described above. Supplementary Table 3 also lists a number of archival detections of PSR J1824–2452I with

the GBT since its discovery[74] as a radio pulsar in 2006. These observations have been acquired as part of a regular timing program of the radio pulsars in M28 (Ransom et al.) and together with archival X-ray observations they conclusively demonstrate that the system has switched between rotation-powered radio pulsar and accretion-powered X-ray pulsar (and back) during 2006–2013.

Table 3: **Abridged Radio/X-ray History of PSR J1824–2452I/IGR J18245–2452**: Flux densities of radio observations were measured at 2.0 GHz (GBT), 1.4 GHz (WSRT/Parkes), and 5.5/9 GHz (ATCA). Radio non detections are marked by a dash in the flux column, and are only moderately constraining as to whether the source was emitting as a radio pulsar at this epoch (see text for details). GBT non-detections prior to 2012-10-07 are not listed. Observed X-ray fluxes are evaluated in the 0.5–10 keV band (20–100 keV for INTEGRAL), and given in mCrab (1Crab = 4.32×10^{-8} erg cm^{-2} s^{-1} in the 0.5–10 keV band).

UT Date	MJD Start	Telescope	Type	Flux	Comments
2002-07-04	52,459.752	Chandra/ACIS–S	X-rays	$(7 \pm 2) \times 10^{-4}$ mCrab	X-ray Quiescence
2002-08-04	52,490.990	Chandra/ACIS–S	X-rays	$(8 \pm 2) \times 10^{-4}$ mCrab	X-ray Quiescence
2002-09-09	52,526.705	Chandra/ACIS–S	X-rays	$(6 \pm 2) \times 10^{-4}$ mCrab	X-ray Quiescence
2002-11-08	52,586.237	Chandra/HRC–S	X-rays	1×10^{-3} mCrab	X-ray Quiescence
2006-01/02	53,738 – 53,781	GBT	Radio		Discovery of PSR J1824–2452I (ref. 69)
2006-05-27	53,882.520	Chandra/HRC–S	X-rays	1×10^{-3} mCrab	X-ray Quiescence
2006/2007		Various GBT Radio Observations			
2007-12-30	54,464.746	GBT	Radio	$\sim 20\,\mu$Jy	Radio Pulsations
2008-04-17	54,573.354	GBT	Radio	$\sim 20\,\mu$Jy	Radio Pulsations
2008-06-13	54,631.274	GBT	Radio	$\sim 20\,\mu$Jy	Radio Pulsations
2008-08-07	54,685.865	Chandra	X-rays	$(14.8 \pm 0.5) \times 10^{-3}$ mCrab	X-ray Enhanced
2008-08-10	54,688.993	Chandra	X-rays	$(10.9 \pm 0.5) \times 10^{-3}$ mCrab	X-ray Enhanced
2009-05-06	54,957.418	GBT	Radio	$\sim 20\,\mu$Jy	Radio Pulsations
2009/2012		Various GBT Radio Observations			
2012-10-07	56,207.967	GBT	Radio	–	–
2013-01-06	56,298.702	GBT	Radio	–	–
2013-03-28	56,379.122	INTEGRAL/ISGRI	X-rays	~ 90 mCrab	Discovery of IGR J18245–2452
2013-03-30	56,381.632	Swift/XRT	X-rays	(19.4 ± 0.2) mCrab	X-ray Outburst / Pulsations
2013-04-04	56,386.018	XMM-Newton/EPIC pn	X-rays	(6.56 ± 0.02) mCrab	X-ray Outburst / Pulsations
2013-04-05	56,387.720	ATCA	Radio	(0.62 ± 0.03) mJy (5.5 GHz)	Non-pulsed
				(0.75 ± 0.04) mJy (9 GHz)	Non-pulsed
2013-04-08	56,390.481	GBT	Radio	–	–

Table 3 – continued from previous page

UT Date	MJD Start	Telescope	Type	Flux	Comments
2013-04-13	56,395.294	XMM-Newton/EPIC pn	X-rays	(6.76 ± 0.02) mCrab	X-ray Outburst / Pulsations
2013-04-15	56,397.469	GBT	Radio	–	–
2013-04-29	56,411.010	Chandra/HRC–S	X-rays [a]	9.5×10^{-3} mCrab	X-ray Enhanced
2013-04-29	56,411.560	Parkes	Radio	–	–
2013-05-01	56,413.557	Swift/XRT	X-rays [a,b]	$(3.8 \pm 1.0) \times 10^{-2}$ mCrab	Latest X-ray detection
2013-05-02	56,414.164	WSRT	Radio	$50 \pm 30\mu$Jy	Radio Pulsations
2013-05-04	56,416.162	WSRT	Radio	–	–
2013-05-06	56,418.170	WSRT	Radio	–	–
2013-05-06	56,418.296	GBT	Radio	–	–
2013-05-06	56,418.831	Swift/XRT	X-rays [a,b]	$< 4 \times 10^{-2}$ mCrab	X-ray non detection
2013-05-07	56,419.114	WSRT	Radio	–	–
2013-05-09	56,421.442	GBT	Radio	–	–
2013-05-10	56,422.544	Parkes	Radio	$60 \pm 30\mu$Jy	Radio Pulsations
2013-05-11	56,423.405	GBT	Radio	$10 \pm 5\mu$Jy	Radio Pulsations
2013-05-13	56,425.432	GBT	Radio	$20 \pm 10\mu$Jy	Radio Pulsations
2013-05-13	56,425.684	Parkes	Radio	$50 \pm 30\mu$Jy	Radio Pulsations
2013-05-18	56,430.277	GBT	Radio	–	–
2013-05-24	56,436.437	GBT	Radio	–	–
2013-05-31	56,443.183	GBT	Radio	–	–

[a] Flux estimated assuming a $\Gamma = 2.5$ power-law spectral shape. [b] Other unresolved sources[60,61] in M28 are expected to give a contribution of $\approx 7 \times 10^{-3}$ mCrab to the quoted flux value/upper limit. Upper limits are evaluated at 3-σ confidence level.

31. Eckert, D. *et al.* IGR J18245-2452: a new hard X-ray transient discovered by INTEGRAL. *Astron. Tel.* **4925**, 1 (2013).

32. Ubertini, P. *et al.* IBIS: The Imager on-board INTEGRAL. *Astron. Astrophys.* **411**, L131–L139 (2003).

33. Lebrun, F. *et al.* ISGRI: The INTEGRAL Soft Gamma-Ray Imager. *Astron. Astrophys.* **411**, L141–L148 (2003).

34. Winkler, C. *et al.* The INTEGRAL mission. *Astron. Astrophys.* **411**, L1–L6 (2003).

35. Harris, W. E. A Catalog of Parameters for Globular Clusters in the Milky Way. *Astron. J.* **112**, 1487–1488 (1996).

36. Lund, N. *et al.* JEM-X: The X-ray monitor aboard INTEGRAL. *Astron. Astrophys.* **411**, L231–L238 (2003).

37. Jansen, F. *et al.* XMM-Newton observatory. I. The spacecraft and operations. *Astron. Astrophys.* **365**, L1–L6 (2001).

38. Strüder, L. *et al.* The European Photon Imaging Camera on XMM-Newton: The pn-CCD camera. *Astron. Astrophys.* **365**, L18–L26 (2001).

39. Turner, M. J. L. *et al.* The European Photon Imaging Camera on XMM-Newton: The MOS cameras : The MOS cameras. *Astron. Astrophys.* **365**, L27–L35 (2001).

40. den Herder, J. W. *et al.* The Reflection Grating Spectrometer on board XMM-Newton. *Astron. Astrophys.* **365**, L7–L17 (2001).

41. Gierliński, M. & Poutanen, J. Physics of accretion in the millisecond pulsar XTE J1751-305. *Mon. Not. R. Astron. Soc.* **359**, 1261–1276 (2005).

42. Papitto, A. *et al.* XMM-Newton detects a relativistically broadened iron line in the spectrum of the ms X-ray pulsar SAX J1808.4-3658. *Astron. Astrophys.* **493**, L39–L43 (2009).

43. Patruno, A. *et al.* SAXJ1808.4-3658: high-resolution spectroscopy and decrease of pulsed fraction at low energies. *Mon. Not. R. Astron. Soc.* **396**, L51–L55 (2009).

44. Papitto, A. *et al.* The X-ray spectrum of the newly discovered accreting millisecond pulsar IGR J17511-3057. *Mon. Not. R. Astron. Soc.* **407**, 2575–2588 (2010).

45. Papitto, A. *et al.* The accretion flow to the intermittent accreting millisecond pulsar, HETE J1900.1-2455, as observed by XMM-Newton and RXTE. *Mon. Not. R. Astron. Soc.* **429**, 3411–3422 (2013).

46. Leahy, D. A., Elsner, R. F. & Weisskopf, M. C. On searches for periodic pulsed emission - The Rayleigh test compared to epoch folding. *Astrophys. J.* **272**, 256–258 (1983).

47. Deeter, J. E., Boynton, P. E. & Pravdo, S. H. Pulse-timing observations of Hercules X-1. *Astrophys. J.* **247**, 1003–1012 (1981).

48. Papitto, A. *et al.* Spin down during quiescence of the fastest known accretion-powered pulsar. *Astron. Astrophys.* **528**, A55 (2011).

49. Makishima, K. *et al.* Simultaneous X-ray and optical observations of GX 339-4 in an X-ray high state. *Astrophys. J.* **308**, 635–643 (1986).

50. Zdziarski, A. A., Johnson, W. N. & Magdziarz, P. Broad-band γ-ray and X-ray spectra of NGC 4151 and their implications for physical processes and geometry. *Mon. Not. R. Astron. Soc.* **283**, 193–206 (1996).

51. Życki, P. T., Done, C. & Smith, D. A. The 1989 May outburst of the soft X-ray transient GS 2023+338 (V404 Cyg). *Mon. Not. R. Astron. Soc.* **309**, 561–575 (1999).

52. Gierliński, M., Done, C. & Barret, D. Phase-resolved X-ray spectroscopy of the millisecond pulsar SAX J1808.4-3658. *Mon. Not. R. Astron. Soc.* **331**, 141–153 (2002).

53. Falanga, M. *et al.* INTEGRAL and RXTE observations of accreting millisecond pulsar IGR J00291+5934 in outburst. *Astron. Astrophys.* **444**, 15–24 (2005).

54. Watson, M. G. *et al.* The XMM-Newton serendipitous survey. V. The Second XMM-Newton serendipitous source catalogue. *Astron. Astrophys.* **493**, 339–373 (2009).

55. Burrows, D. N. *et al.* The Swift X-Ray Telescope. *Sp. Sc. Rev.* **120**, 165–195 (2005).

56. Gehrels, N. *et al.* The Swift Gamma-Ray Burst Mission. *Astrophys. J.* **611**, 1005–1020 (2004).

57. Barthelmy, S. D. *et al.* The Burst Alert Telescope (BAT) on the SWIFT Midex Mission. *Sp. Sc. Rev.* **120**, 143–164 (2005).

58. Romano, P. *et al.* Swift observations of IGR J18245-2452. *Astron. Tel.* **4929**, 1 (2013).

59. Heinke, C. O., Bahramian, A., Wijnands, R. & Altamirano, D. IGR J18245-2452 is a new transient located in the core of the globular cluster M28. *Astron. Tel.* **4927**, 1 (2013).

60. Becker, W. *et al.* Chandra X-Ray Observatory Observations of the Globular Cluster M28 and Its Millisecond Pulsar PSR B1821-24. *Astrophys. J.* **594**, 798–811 (2003).

61. Bogdanov, S. *et al.* Chandra X-ray Observations of 12 Millisecond Pulsars in the Globular Cluster M28. *Astrophys. J.* **730**, 81 (2011).

62. Linares, M. IGR J18245-2452: an accreting neutron star and thermonuclear burster in M28. *Astron. Tel.* **4960**, 1 (2013).

63. Lewin, W. H. G., van Paradijs, J. & Taam, R. E. X-Ray Bursts. *Sp. Sc. Rev.* **62**, 223–389 (1993).

64. Watts, A. L. Thermonuclear Burst Oscillations. *Annu. Rev. Astron. Astr.* **50**, 609–640 (2012).

65. Patruno, A. Burst oscillations in the X-ray binary IGR J18245-2452 in M28. *Astron. Tel.* **5068**, 1 (2013).

66. Riggio, A. *et al.* Coherent pulsations and burst oscillations in the millisecond pulsar IGR J18245-2452/PSR J1824-2452I in M28 . *Astron. Tel.* **5086**, 1 (2013).

67. Zombeck, M. V. *et al.* High-resolution camera (HRC) on the Advanced X-Ray Astrophysics Facility (AXAF). In *Society of Photo-Optical Instrumentation Engineers (SPIE) Conference Series, Vol. 2518* (1995).

68. Garmire, G. P., Bautz, M. W., Ford, P. G., Nousek, J. A. & Ricker, G. R., Jr. Advanced CCD imaging spectrometer (ACIS) instrument on the Chandra X-ray Observatory. In *Society of Photo-Optical Instrumentation Engineers (SPIE) Conference Series, Vol. 4851* (2003).

69. Anders, E. & Grevesse, N. Abundances of the elements - Meteoritic and solar. *Geochim. Cosmochim. A.* **53**, 197–214 (1989).

70. Balucinska-Church, M. & McCammon, D. Photoelectric absorption cross sections with variable abundances. *Astrophys. J.* **400**, 699–700 (1992).

71. Sault, R., Teuben, P. & Wright, M. A retrospective view of miriad. *ASP Conf. Ser.* **77**, 433–436 (1995).

72. Gaensler, B. M., Stappers, B. W. & Getts, T. J. Transient Radio Emission from SAX J1808.4-3658. *Astrophys. J.* **522**, L117–L119 (1999).

73. van Straten, W. & Bailes, M. DSPSR: Digital Signal Processing Software for Pulsar Astronomy. *Publ. Astr. Soc. Austr.* **28**, 1–14 (2011).

74. Bégin, S. *A search for fast pulsars in globular clusters*. Master of science, The Faculty of Graduate Studies (Physics), The University of British Columbia (2006).

75. Dewey, R. J., Taylor, J. H., Weisberg, J. M. & Stokes, G. H. A search for low-luminosity pulsars. *Astrophys. J.* **294**, L25–L29 (1985).

76. Karuppusamy, R., Stappers, B. & van Straten, W. PuMa-II: A Wide Band Pulsar Machine for the Westerbork Synthesis Radio Telescope. *Publ. Astr. Soc. Pac.* **120**, 191–202 (2008).

77. DuPlain, R. *et al.* Launching GUPPI: the Green Bank Ultimate Pulsar Processing Instrument. In *Society of Photo-Optical Instrumentation Engineers (SPIE) Conference Series*, vol. 7019 of *Society of Photo-Optical Instrumentation Engineers (SPIE) Conference Series* (2008).